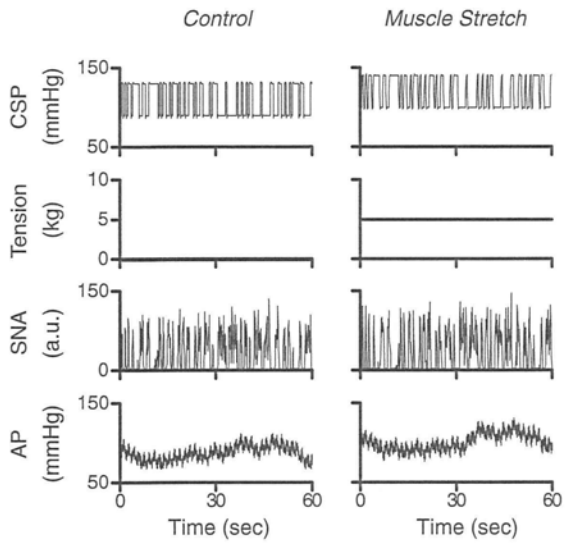

Fig. 1. Typical time series of intracarotid sinus pressure (CSP), muscle tension, sympathetic nerve activity [SNA; in arbitrary units (au)], and arterial pressure (AP) under control (*left*) and muscle stretch (*right*) conditions. CSP was perturbed according to a binary white noise sequence. Muscle stretch increased mean levels of SNA and AP under muscle stretch conditions compared with the control conditions.

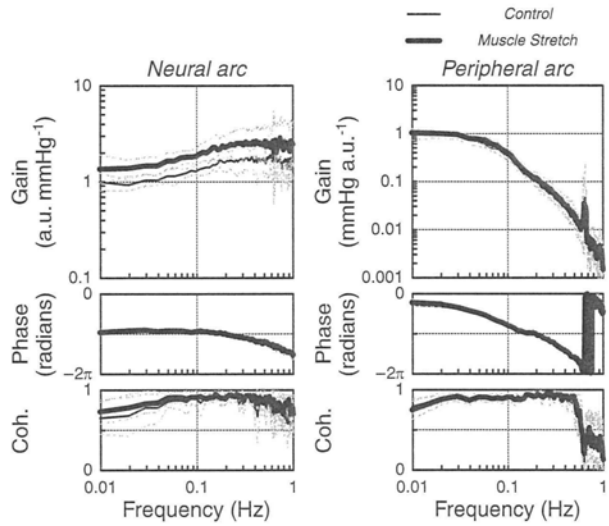

Fig. 2. Transfer functions of the neural (*left*) and peripheral (*right*) arcs under control and muscle stretch conditions. In the neural arc, the input was CSP and the output was SNA. In the peripheral arc, the input was SNA and the output was AP. The mean level of CSP input to the neural arc was set higher under muscle stretch conditions than under control conditions to mimic the physiological condition (i.e., baroreflex closed-loop conditions). Gain plots (*top*), phase plots (*middle*) and coherence (Coh) functions (*bottom*) are shown. Thin and thick solid lines indicate control and muscle stretch conditions, respectively. In the neural arc (*left*), muscle stretch caused an approximately parallel upward shift of the gain plot. Solid and dashed lines represent means and means ± SD values, respectively.

the frequency of input modulation increased under both conditions, indicating derivative characteristics of the neural arc. Muscle stretch caused an approximately parallel upward shift of the gain plot. The phase approached $-\pi$ radians ($-180°$) at the lowest frequency (0.01 Hz) under both conditions, reflecting the negative feedback character of the baroreflex neural arc (i.e., an increase in CSP decreased SNA). Phase plots were nearly superimposed between the two conditions. Coherence values did not differ between both conditions. In the peripheral arc, the dynamic gain decreased in the frequency range from 0.05 to 1 Hz as the frequency of input modulation increased under both conditions, indicating the low-pass characteristics of the peripheral arc. The phase approached 0 radians at the lowest frequency (0.01 Hz) under both conditions, reflecting the fact that an increase in SNA increased AP. The phase lagged with increasing frequency up to 1 Hz. The gain plot, phase plot, and Coh(f) did not differ between both conditions.

Table 2 summarizes gains of the transfer functions. In the neural arc, $G_{0.01}$, $G_{0.1}$, $G_{0.5}$, and G_1 were higher under muscle

Table 1. *Mean levels and CVs of CSP, SNA, and AP at 1, 2, 4, and 6 min under control and muscle stretch conditions*

	Time			
	1 min	2 min	4 min	6 min
		CSP		
Control	95±18	96±18	95±18	96±18
CV	13±2	12±3	11±3	14±2
Muscle stretch	114±15*	115±16*	113±16*	114±15*
CV	11±2	11±1	10±2	12±2
		SNA		
Control	102±4	99±5	100±4	99±4
CV	46±11	45±9	43±9	47±9
Muscle stretch	133±22*	129±21*	127±17*	126±17*
CV	48±11	47±8	44±9	49±10
		AP		
Control	90±21	89±20	88±16	88±18
CV	7±2	6±2	6±2	6±2
Muscle stretch	107±26*	105±22*	104±15*	101±15*
CV	7±3	6±3	6±3	7±2

Values are means ± SD; $n = 7$. CSP, carotid sinus pressure (in mmHg); SNA, sympathetic nerve activity (in %); AP, arterial pressure (in mmHg); CV, coefficient of variation. Mean and CV values were calculated from 30-s data ending at each time point. *$P < 0.05$ vs. control.

Table 2. *Gains of the transfer functions*

	Control	Muscle Stretch
Neural arc		
$G_{0.01}$, au/mmHg	1.01±0.23	1.44±0.56*
$G_{0.1}$, au/mmHg	1.30±0.11	1.86±0.37*
$G_{0.5}$, au/mmHg	1.77±0.64	2.65±1.08*
G_1, au/mmHg	1.72±0.66	2.72±1.40*
Peripheral arc		
$G_{0.01}$, mmHg/au	1.08±0.06	1.06±0.20
$G_{0.1}$, mmHg/au	0.37±0.09	0.42±0.09
$G_{0.5}$, mmHg/au	0.02±0.01	0.02±0.01
G_1, mmHg/au	0.004±0.001	0.004±0.002
Total loop		
$G_{0.01}$, mmHg/mmHg	1.08±0.18	1.53±0.63*
$G_{0.1}$, mmHg/mmHg	0.48±0.12	0.81±0.31*
$G_{0.5}$, mmHg/mmHg	0.04±0.04	0.06±0.04*
G_1, mmHg/mmHg	0.006±0.003	0.013±0.013

Values are means ± SD; $n = 7$. $G_{0.01}$, $G_{0.1}$, $G_{0.5}$, and G_1, dynamic gains at 0.01, 0.1, 0.5, and 1 Hz, respectively; au, arbitrary units. *$P < 0.05$ vs. control.

stretch compared with control conditions. In the peripheral arc, $G_{0.01}$, $G_{0.1}$, $G_{0.5}$, and G_1 were unchanged between control and muscle stretch conditions.

Figure 3 shows the total baroreflex loop transfer functions (CSP to AP) under control and muscle stretch conditions. The thin and thick solid lines in Fig. 3 indicate control and muscle stretch conditions, respectively. The dynamic gain decreased as the frequency of input modulation increased under both conditions, indicating low-pass characteristics. The dynamic gain under muscle stretch conditions was higher than that under control conditions in frequency from 0.01 to 0.5 Hz (Table 2). The phase plot and Coh(*f*) did not differ between both conditions.

Figure 4 shows step responses of SNA corresponding to the transfer functions in the neural arc shown in Fig. 2. The initial drop in the SNA response as well as the steady-state response was augmented during muscle stretch (Table 3). T_{peak} did not differ between control and muscle stretch conditions (Table 3).

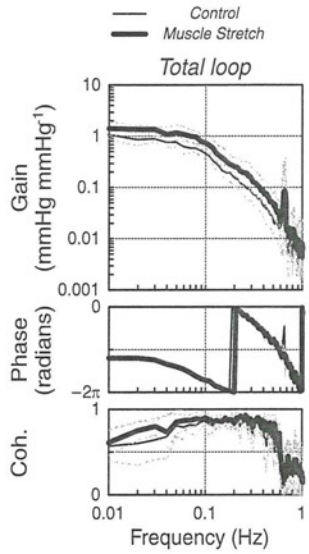

Fig. 3. Total loop transfer functions from CSP to AP under control and muscle stretch conditions. Gain plots (*top*), phase plots (*middle*) and coherence functions (*bottom*) are shown. Thin and thick solid lines indicate control and muscle stretch conditions, respectively. The dynamic gain decreased as the frequency of input modulation increased under both conditions, indicating low-pass characteristics. Muscle stretch caused an approximately parallel upward shift of the gain plot. Solid and dashed lines represent means and means ± SD values, respectively.

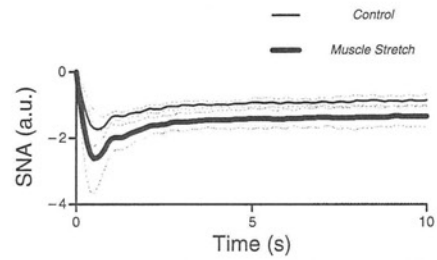

Fig. 4. Step responses corresponding to transfer functions of the neural arc obtained from Fig. 2, showing the SNA response to a 1-mmHg increase in input pressure. Thin and thick solid lines indicate control and muscle stretch conditions, respectively. The initial drop in the SNA response as well as the steady-state response was augmented by the muscle stretch. Solid and dashed lines represent means and means ± SD values, respectively.

DISCUSSION

The key new findings of the present study are as follows. Muscle stretch increased the dynamic gain of the carotid sinus baroreflex neural arc as estimated by binary white noise input (Fig. 2). In contrast, the peripheral arc transfer function remained unchanged irrespective of the muscle stretch (Fig. 2). These results suggest that during muscle mechanoreflex activation, the dynamic SNA response to CSP perturbation is augmented.

System identification by the white noise approach. To identify the dynamic characteristics of arterial baroreflex function quantitatively, we described the carotid sinus baroreflex control of SNA and AP in terms of system identification using the white noise technique. Compared with the traditional approach of testing dynamic properties of the physiological system with step and sine wave stimuli, the white noise approach has definite advantages, as follows (27). First, if a step stimulus is applied, we learn the response of the system to this step and have little notion of the response of the system to any other type of stimulus. If a sinusoidal pulse is applied, then we know the response of the system to such a stimulus and little else. The same applies for any other specific waveform. Theoretically speaking, the system is tested with every possible stimulus in the white noise approach. The white noise stimulus is a very rich stimulus. It should be emphasized that the white noise method is perfectly suited to the analysis of linear systems. As shown in Figs. 2 and 3, high coherence values close to unity indicate the validity of our method for system identification. Second, the identification of the physiological system through the white noise technique is largely unaffected by the types of contaminating noise usually present in such a system. Our study provides the first and quantitative description of the dynamic characteristics of the carotid sinus baroreflex during isolated activation of mechanosensitive afferents from skeletal muscle.

Effects of the muscle mechanoreflex on dynamic characteristics of the carotid sinus baroreflex. The effects of activation of afferents from skeletal muscle, such as those occurring during exercise, on the arterial baroreflex have been extensively studied (5, 13, 29, 42, 43, 49, 58, 59). These studies have demonstrated that the afferent input from muscle resets the baroreflex control of AP, heart rate, and SNA. However, the dynamic characteristics of the arterial baroreflex during isolated activation of muscle mechanosensitive afferents have never been analyzed. In the present study, muscle stretch increased dynamic gain in every frequency (Fig. 2 and Table

Table 3. *Parameters of step responses*

	Control	Muscle Stretch
S_{50}, au	−1.05±0.30	−1.69±0.69*
S_{peak}, au	−2.10±0.50	−3.08±1.45*
T_{peak}, s	0.63±0.21	0.64±0.20

Values are means ± SD; n = 7. A step response is defined as a SNA response to a 1-mmHg change in input pressure. S_{50}, step response at 50 s; S_{peak}, negative peak response; T_{peak}, time to negative peak. *$P < 0.05$ vs. control.

2), whereas it did not affect the peripheral arc. These data are the first to provide quantitative evidence demonstrating that the dynamic SNA response to CSP perturbation is augmented during isolated activation of the muscle mechanoreflex. Although an increase in dynamic gain in the lowest frequency (0.01 Hz) was expected from the results of our previous studies showing an increase in static gain by muscle stretch (58, 59), the information was insufficient to perform a simulation study to examine the effects of muscle stretch on the closed-loop dynamic AP regulation (see *Physiological implications*). The present study extended our previous work by providing additional information on the dynamic interaction over a wide range of frequencies between 0.01 and 1 Hz in the carotid sinus baroreflex.

The static characteristics of the arterial baroreflex determine an operating point of the baroreflex system. Furthermore, the static characteristics described by a modeled sigmoid function provide the parameters of threshold, saturation, and maximal gain at the centering point. However, the static characteristics alone cannot provide the information on the changes over time in the response of the baroreflex system. On the other hand, dynamic analysis techniques such as transfer function analysis estimated by the white noise approach provide information on the stability and quickness of the system response. The dynamic SNA response to baroreceptor pressure input became greater as the frequency of input modulation increased, suggesting derivative characteristics (i.e., high-pass characteristics) of the baroreflex neural arc (Fig. 2, *left*, thin solid line). In contrast, the dynamic AP response to SNA became smaller as the frequency of SNA modulation increased, indicating low-pass characteristics of the baroreflex peripheral arc (Fig. 2, *right*, thin solid line). The total loop transfer function (CSP to AP) is determined by a product of the neural and peripheral arc transfer functions (Fig. 3, thin solid line). Therefore, the decreasing slope of dynamic gain in the total loop transfer function was shallower than that in the corresponding peripheral arc. In other words, the fast neural arc effectively compensates for the slow peripheral arc to accelerate dynamic AP regulation by the baroreflex negative-feedback loop (14). During muscle stretch, the dynamic gain in the neural arc was increased by ~50% in every frequency under study (Fig. 2 and Table 2), indicating that the derivative characteristics of the neural arc were maintained. As a result, the effect of the neural arc compensating for the slow AP response was preserved during the activation of muscle mechanoreflex (Fig. 3 and Table 2). Furthermore, the total loop dynamic gain was augmented during the muscle stretch due to the upward shift of the neural arc transfer function.

Because we used passive muscle stretch as the input for the muscle mechanoreflex, the physiological significance of the present results should be interpreted carefully. Several studies have examined the arterial baroreflex control of SNA during static and dynamic exercise. Static and heavy dynamic exercise resets the baroreflex control of SNA to higher SNA levels with an increase in its sensitivity (9, 11, 17, 32). On the other hand, mild to moderate dynamic exercise resets the baroreflex control of SNA without any change in its sensitivity (3, 24, 38). Because the muscle mechanoreflex is activated during mild to moderate dynamic exercise (4), our results indicate that the muscle mechanoreflex may contribute to increasing the baroreflex gain of SNA during mild to moderate dynamic exercise. In addition to differences in the measured SNA (renal vs. muscle), analytic methods of baroreflex function, modes of mechanoreflex activation, and/or species between the present study and previous studies, the cardiopulmonary baroreflex should be taken into account. Charkoudian et al. (1) demonstrated that increasing central venous pressure via head-down tilt or saline infusion attenuated the baroreflex sensitivity in the control of SNA. The activation of cardiopulmonary baroreceptors induced by increasing central venous pressure may influence the arterial baroreflex control during dynamic exercise (37). In the present study, however, the cardiopulmonary baroreflex did not operate due to bilateral vagotomy.

Previous studies (7, 25) have suggested that the muscle mechanoreflex has a dominant role in pressor reflexes during muscle contraction in anesthetized or decerebrate cats. Although we believe that the mechanoreflex is one of the pressor reflexes during exercise, the functional importance of the muscle mechanoreflex in cardiovascular regulation during exercise in conscious conditions is debatable. Matsukawa et al. (28) recently reported that blockade of the muscle mechanoreflex by gadolinium did not alter AP responses to isometric exercise in conscious cats. Moreover, they found that gadolinium significantly diminished the pressor responses to passive muscle stretch in anesthetized cats. These observations suggest that, under the experimental design, the muscle mechanoreflex would not be activated during exercise or, even if it was activated, it has no functional importance in cardiovascular responses to exercise in conscious conditions. One criticism for the study is that there is always a possibility that changes in the central command in conscious conditions had compensated for the lack of muscle mechanoreflex. Further studies are needed to better understand the role of the muscle mechanoreflex on neural cardiovascular responses during exercise.

High-pass characteristics of the baroreflex neural arc. It is likely that the dynamic characteristics of the baroreflex neural arc actually reflect the intrinsic and synaptic properties of central nervous system neurons and neural circuits that transmit baroreceptor input. However, the central baroreceptor synapses are characterized as a low-pass filter (26). The difference between high-pass characteristics of the neural arc transfer gain and low-pass characteristics of the central baroreceptor synaptic transmission could be attributable to the difference of estimated frequency ranges. Frequency-dependent depression (FFD) of synaptic transmission in the baroreflex central pathways is the phenomenon that the probability of excitatory postsynaptic potentials progressively reduces as the frequency of afferent input increases beyond 1 Hz (2, 33). Although FDD and transfer gain should be discriminated in theory, interactions between FDD and transfer gain may occur when the modulation frequency of afferent fiber stimulation approached the frequency range of FDD. Indeed, Kawada et al. (23) found high-cut characteristics of the baroreflex neural arc in the frequency range above ~1 Hz. In the present study, the transfer gain was derived from 0.01 to 1 Hz. Whether the dynamic interaction between carotid sinus baroreflex and muscle mechanoreflex exists in the frequency range beyond 1 Hz awaits further studies.

Part of the high-pass characteristics in the baroreflex neural arc is attributable to the derivative nature observed in the baroreceptor transduction from CSP input to baroreceptor afferent nerve activity (i.e., mechanoneural transduction) (21).

However, we think there exists high-pass characteristics in the transduction from baroreceptor afferent input to efferent SNA, because the magnitude of high-pass characteristics slightly differs between cardiac and renal SNAs in response to the same baroreceptor pressure perturbation (18).

In an electrical circuit, we can design a high-pass filter only from low-pass filter elements using a feedback loop (Fig. 5). Although the main forward path of the baroreflex neural arc from afferent nerve activity to efferent SNA is considered to be the nucleus tructus solitarius, caudal ventrolateral medulla, and rostral ventrolateral medulla (53), there could be feedback connections between these areas. Therefore, it is possible that synaptic connection has basically low-pass characteristics, whereas the baroreflex neural arc reveals high-pass characteristics as a neural circuit. The speculation also needs to be verified experimentally in the future.

Physiological implications. Under physiological conditions, the baroreflex is closed as a negative feedback system. In the following discussion, we will focus on the effect of the augmentation of dynamic SNA modulation in the neural arc on the closed-loop dynamic AP regulation. Figure 6*A* illustrates a simulator consisting of the linear neural arc transfer function (H_N) and linear peripheral arc transfer function (H_P) followed by the nonlinear sigmoidal components (see the APPENDIX for details). A closed-loop AP response to a stepwise pressure perturbation (−40 mmHg) with pulsatile pressure was simulated, and the result is shown in Fig. 6*B*. Muscle stretch shortened the time to 95% of steady state by ~33% from 7.2 to 4.8 s (shaded and solid arrows in Fig. 6*B*). This result suggests that, under baroreflex closed-loop conditions, the rate of recovery in AP following a pressure perturbation occurs sooner when accompanied by the muscle mechanoreflex. Increasing the quickness of the negative-feedback system can be caused by augmentation and/or acceleration of the open-loop transfer function of the system. In our baroreflex open-loop experiment, S_{50} and S_{peak} in the step responses of SNA were augmented by the muscle stretch (Fig. 4 and Table 3). On the other hand, T_{peak} did not differ between control and muscle stretch conditions (Fig. 4 and Table 3). These results suggest that the improvement in the quickness of the AP restoration via the baroreflex observed in the closed-loop simulation was induced by augmentation, rather than acceleration, of the dynamic SNA response in the neural arc. However, further experimental studies are needed to verify the simulation model.

Limitations. The present study has several limitations. First, we performed the experiment in anesthetized animals. Previous studies have suggested that any anesthetic could alter the baroreflex regulation in AP (54–56). The gain of the baroreflex is reported in the conscious state to be higher (~2-fold) than in the anesthetized state. A previous study (52) suggested that α-chloralose anesthesia could alter the dynamic characteristics of the baroreflex regulation around the frequency of 5 Hz. However, the anesthesia was convenient for the elimination of the central command. Furthermore, we compared the baroreflex gain between muscle stretch and nonstretch conditions both under anesthesia. Therefore, a reasonable interpretation would be that the increased baroreflex gain is attributable to muscle stretch in this experiment.

Second, stretching of skeletal muscle provides a stimulus for the activation of mechanoreceptors that is different from that which occurs during muscle contraction. During contraction, mechanoreceptors are activated by a shortening of skeletal muscle and by compression of the receptors. Thus, mechanoreceptors may be stimulated in a very different manner during stretch, which would likely affect the magnitude of the corresponding reflex response. In addition, the level of muscle stretch used in our experiment was relatively high (50). The stretch may activate different afferents than contraction (8). Furthermore, the discharge profile of mechanosensitive afferents adapt during static muscle stretch (31). Accordingly, during the muscle stretch for 6 min in the present study, the firing level from the mechanoreceptors might have been

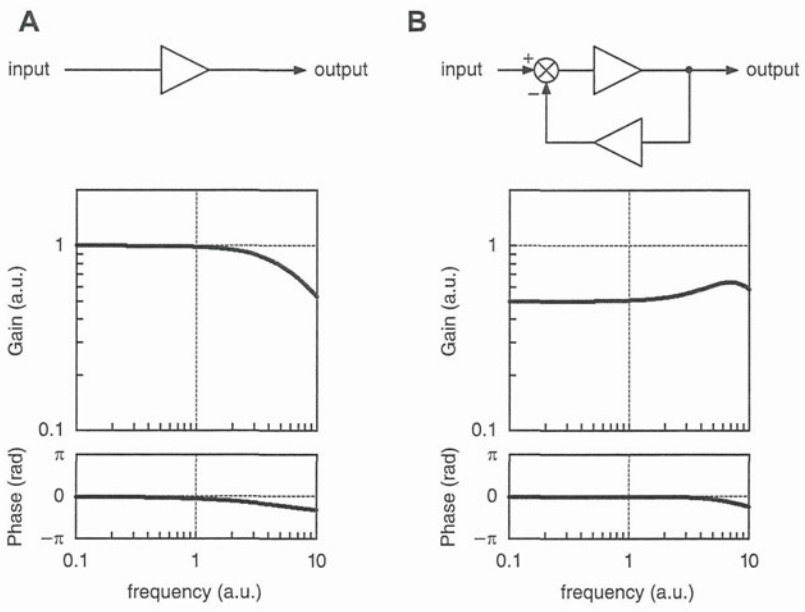

Fig. 5. An example that a circuit consisting of only low-pass elements yields high-pass characteristics as a circuit. *A*: block diagram of a single low-pass element (triangle) and its transfer function. Units for gain and frequency are arbitrary. *B*: block diagram of a circuit with a negative feedback loop with the same low-pass element (triangles). Because gain in the lower frequency range is attenuated more by the low-pass characteristics of the feedback path, the transfer function from input to output reveals high-pass characteristics.

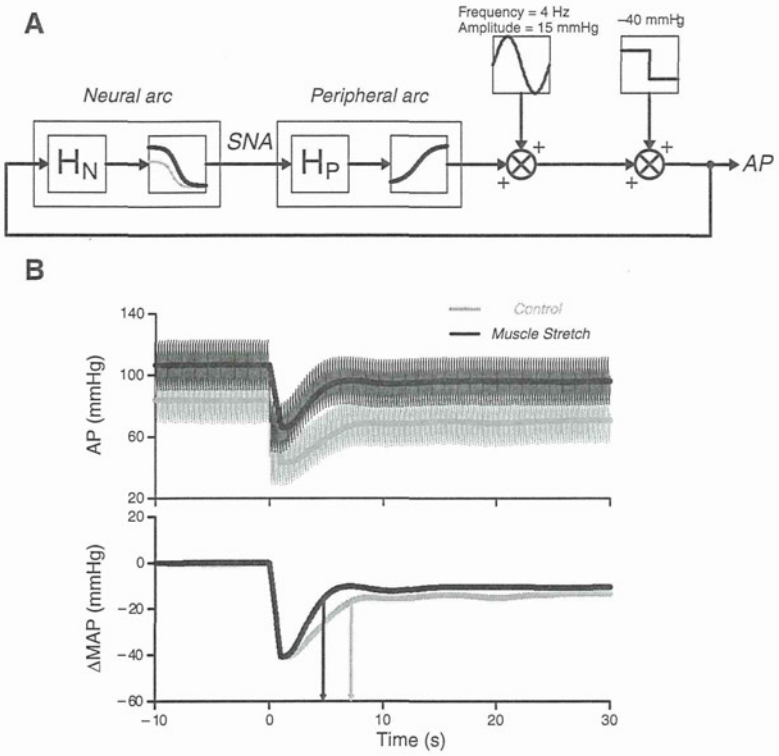

Fig. 6. *A*: simulator of the baroreflex system during activation of the muscle mechanoreflex. A stepwise perturbation with pulsatile pressure was applied to the baroreflex negative feedback system (see the APPENDIX for details). H_N, neural arc transfer function; H_P, peripheral arc transfer function. *B*: simulation results of the closed-loop AP response to the stepwise pressure perturbation (−40 mmHg). Muscle stretch shortened the time to 95% of steady state by ~33% (shaded and solid arrows). Shaded and solid thick lines indicate mean AP (MAP) resampled at 1 Hz. ΔMAP, change in MAP from baseline.

steadily diminishing. In fact, the increase in SNA and AP induced by muscle stretch gradually decreased from 90 s to 6 min after the initiation of the muscle stretch, which was used for data analysis (Table 1). However, SNA and AP remained significantly higher under muscle stretch conditions than control conditions over the protocol for 6 min. Thus, we believe that the mechanoreflex remained activated in this protocol. Further studies are required to elucidate the dynamic interactions between baroreflex and mechanoreflex induced by different modes of activation, such as cyclic activation of the mechanoreflex.

Third, the transfer function analysis is useful in identifying the linear input-output relationship of the baroreflex at a given operating point. However, the transfer function cannot characterize the nonlinear input-output relationship of the system. In the presence of nonlinear system behavior such as the baroreflex system, the transfer function analysis is partly compromised, indicating that the absolute output values of the nonlinear system to given input signals cannot be predicted accurately by the transfer function alone. Combining a linear transfer function with a nonlinear sigmoidal element would increase the accuracy to reproduce dynamic characteristics observed in the baroreflex neural arc (20, 22).

Finally, we measured renal SNA as a proxy of systemic sympathetic activity. SNAs to different organs may vary a lot. Although static and dynamic regulations of the baroreflex neural arc are similar among renal, cardiac, and muscle SNAs (15, 16, 18), whether this holds true during muscle stretch remains to be verified. Also, subsystems of the peripheral arc transfer function such as those relating cardiac output and peripheral vascular resistance remain to be identified.

Conclusions. In conclusion, baroreflex open-loop transfer function analysis demonstrated that the activation of mechanosensitive afferents from skeletal muscles augmented the dynamic SNA response in the neural arc. This augmentation of the dynamic SNA response with maintained derivative characteristics of the neural arc may accelerate closed-loop AP regulation via the baroreflex.

APPENDIX

To simulate the closed-loop AP response to stepwise pressure perturbation (Fig. 6), we used the derivative-sigmoidal cascade model. The cascade model consists of a linear derivative filter followed by a nonlinear sigmoidal component (20, 22).

We modeled the sigmoidal nonlinearity in the baroreflex neural arc interacting with the muscle mechanoreflex by the following four-parameter logistic function with threshold according to a previous study (59):

$$y = \max\left\{\frac{P_1}{1 + \exp[P_2(x - P_3)]} + P_4,\quad \mathrm{Th}\right\} \qquad (A1)$$

where x and y are input (in mmHg) and output (in au) values. P_1 denotes the response range (in au), P_2 is the coefficient of gain, P_3 is the midpoint of the input range (in mmHg), P_4 is the minimum output value of the symmetric sigmoid curve (in au), and Th is a threshold value for the output (in au). The function $\max\{a,b\}$ gives the greater or equal value between a and b. We set $P_1 = 135$ au, $P_2 = 0.13$, $P_3 = 110$ mmHg, $P_4 = -40$ au, and Th = 0 au. Under muscle stretch conditions, the value of P_4 was changed to 5 au. These settings were determined based on the static interaction

between the baroreflex and muscle mechanoreflex obtained from previous studies (58, 59).

The sigmoidal nonlinearity in the peripheral arc was modelled by a four-parameter logistic function as follows:

$$z = \frac{Q_1}{1 + \exp[Q_2(y - Q_3)]} + Q_4 \qquad (A2)$$

where y and z are input (in au) and output (in mmHg) values. Q_1 denotes the response range (in mmHg), Q_2 is the coefficient of gain, Q_3 is the midpoint of the input range (in au), and Q_4 is the minimum output value (in mmHg). We set $Q_1 = 120$ mmHg, $Q_2 = -0.05$, $Q_3 = 70$ au, and $Q_4 = 30$ mmHg under both conditions, according to a previous study (58).

The neural arc (H_N) and peripheral arc (H_P) linear transfer functions under control and muscle stretch conditions were obtained from Fig. 2. Because absolute values of the steady-state gains in the neural and peripheral arcs were determined by a sigmoid curve (*Eqs. A1* and *A2*), the steady-state gains of H_N and H_P under both conditions were normalized to unity.

The input amplitude of the stepwise pressure perturbation was −40 mmHg. To mimic pulsatile pressure, we imposed a sinusoidal input on the output from the peripheral arc. The frequency and zero to peak amplitude of the sinusoidal input were 4 Hz and 15 mmHg, respectively (Fig. 6*A*). The closed-loop AP response was simulated up to 30 s (Fig. 6*B*).

GRANTS

This work was supported by Ministry of Health, Labour and Welfare of Japan Health and Labour Sciences Research Grant for Research on Advanced Medical Technology, Health and Labour Sciences Research Grant for Research on Medical Devices for Analyzing, Supporting and Substituting the Function of Human Body, and Health and Labour Sciences Research Grants H18-Iryo-Ippan-023 and H18-Nano-Ippan-003; the Industrial Technology Research Grant Program of the New Energy and Industrial Technology Development Organization of Japan; and Ministry of Education, Culture, Sports, Science and Technology Grant-In-Aid for Scientific Research 18591992.

REFERENCES

1. **Charkoudian N, Martin EA, Dinenno FA, Eisenach JH, Dietz NM, Joyner MJ.** Influence of increased central venous pressure on baroreflex control of sympathetic activity in humans. *Am J Physiol Heart Circ Physiol* 287: H1658–H1662, 2004.
2. **Chen CY, Horowitz JM, Bonham AC.** A presynaptic mechanism contributes to depression of autonomic signal transmission in NTS. *Am J Physiol Heart Circ Physiol* 277: H1350–H1360, 1999.
3. **Fadel PJ, Ogoh S, Watenpaugh DE, Wasmund W, Olivencia-Yurvati A, Smith ML, Raven PB.** Carotid baroreflex regulation of sympathetic nerve activity during dynamic exercise in humans. *Am J Physiol Heart Circ Physiol* 280: H1383–H1390, 2001.
4. **Gallagher KM, Fadel PJ, Smith SA, Norton KH, Querry RG, Olivencia-Yurvati A, Raven PB.** Increases in intramuscular pressure raise arterial blood pressure during dynamic exercise. *J Appl Physiol* 91: 2351–2358, 2001.
5. **Gallagher KM, Fadel PJ, Stromstad M, Ide K, Smith SA, Querry RG, Raven PB, Secher NH.** Effects of exercise pressor reflex activation on carotid baroreflex function during exercise in humans. *J Physiol* 533: 871–880, 2001.
6. **Gallagher KM, Fadel PJ, Stromstad M, Ide K, Smith SA, Querry RG, Raven PB, Secher NH.** Effects of partial neuromuscular blockade on carotid baroreflex function during exercise in humans. *J Physiol* 533: 861–870, 2001.
7. **Hayes SG, Kaufman MP.** Gadolinium attenuates exercise pressor reflex in cats. *Am J Physiol Heart Circ Physiol* 280: H2153–H2161, 2001.
8. **Hayes SG, Kindig AE, Kaufman MP.** Comparison between the effect of static contraction and tendon stretch on the discharge of group III and IV muscle afferents. *J Appl Physiol* 99: 1891–1896, 2005.
9. **Ichinose M, Saito M, Fujii N, Ogawa T, Hayashi K, Kondo N, Nishiyasu T.** Modulation of the control of muscle sympathetic nerve activity during incremental leg cycling. *J Physiol* 586: 2753–2766, 2008.
10. **Ichinose M, Saito M, Kondo N, Nishiyasu T.** Time-dependent modulation of arterial baroreflex control of muscle sympathetic nerve activity during isometric exercise in humans. *Am J Physiol Heart Circ Physiol* 290: H1419–H1426, 2006.
11. **Ichinose M, Saito M, Wada H, Kitano A, Kondo N, Nishiyasu T.** Modulation of arterial baroreflex control of muscle sympathetic nerve activity by muscle metaboreflex in humans. *Am J Physiol Heart Circ Physiol* 286: H701–H707, 2004.
12. **Ichinose M, Saito M, Wada H, Kitano A, Kondo N, Nishiyasu T.** Modulation of arterial baroreflex dynamic response during muscle metaboreflex activation in humans. *J Physiol* 544: 939–948, 2002.
13. **Iellamo F, Legramante JM, Raimondi G, Peruzzi G.** Baroreflex control of sinus node during dynamic exercise in humans: effects of central command and muscle reflexes. *Am J Physiol Heart Circ Physiol* 272: H1157–H1164, 1997.
14. **Ikeda Y, Kawada T, Sugimachi M, Kawaguchi O, Shishido T, Sato T, Miyano H, Matsuura W, Alexander J Jr, Sunagawa K.** Neural arc of baroreflex optimizes dynamic pressure regulation in achieving both stability and quickness. *Am J Physiol Heart Circ Physiol* 271: H882–H890, 1996.
15. **Kamiya A, Kawada T, Yamamoto K, Michikami D, Ariumi H, Miyamoto T, Shimizu S, Uemura K, Aiba T, Sunagawa K, Sugimachi M.** Dynamic and static baroreflex control of muscle sympathetic nerve activity (SNA) parallels that of renal and cardiac SNA during physiological change in pressure. *Am J Physiol Heart Circ Physiol* 289: H2641–H2648, 2005.
16. **Kamiya A, Kawada T, Yamamoto K, Michikami D, Ariumi H, Miyamoto T, Uemura K, Sugimachi M, Sunagawa K.** Muscle sympathetic nerve activity averaged over 1 minute parallels renal and cardiac sympathetic nerve activity in response to a forced baroreceptor pressure change. *Circulation* 112: 384–386, 2005.
17. **Kamiya A, Michikami D, Fu Q, Niimi Y, Iwase S, Mano T, Suzumura A.** Static handgrip exercise modifies arterial baroreflex control of vascular sympathetic outflow in humans. *Am J Physiol Regul Integr Comp Physiol* 281: R1134–R1139, 2001.
18. **Kawada T, Shishido T, Inagaki M, Tatewaki T, Zheng C, Yanagiya Y, Sugimachi M, Sunagawa K.** Differential dynamic baroreflex regulation of cardiac and renal sympathetic nerve activities. *Am J Physiol Heart Circ Physiol* 280: H1581–H1590, 2001.
19. **Kawada T, Shishido T, Inagaki M, Zheng C, Yanagiya Y, Uemura K, Sugimachi M, Sunagawa K.** Estimation of baroreflex gain using a baroreflex equilibrium diagram. *Jpn J Physiol* 52: 21–29, 2002.
20. **Kawada T, Uemura K, Kashihara K, Kamiya A, Sugimachi M, Sunagawa K.** A derivative-sigmoidal model reproduces operating point-dependent baroreflex neural arc transfer characteristics. *Am J Physiol Heart Circ Physiol* 286: H2272–H2279, 2004.
21. **Kawada T, Yamamoto K, Kamiya A, Ariumi H, Michikami D, Shishido T, Sunagawa K, Sugimachi M.** Dynamic characteristics of carotid sinus pressure-nerve activity transduction in rabbits. *Jpn J Physiol* 55: 157–163, 2005.
22. **Kawada T, Yanagiya Y, Uemura K, Miyamoto T, Zheng C, Li M, Sugimachi M, Sunagawa K.** Input-size dependence of the baroreflex neural arc transfer characteristics. *Am J Physiol Heart Circ Physiol* 284: H404–H415, 2003.
23. **Kawada T, Zheng C, Yanagiya Y, Uemura K, Miyamoto T, Inagaki M, Shishido T, Sugimachi M, Sunagawa K.** High-cut characteristics of the baroreflex neural arc preserve baroreflex gain against pulsatile pressure. *Am J Physiol Heart Circ Physiol* 282: H1149–H1156, 2002.
24. **Keller DM, Fadel PJ, Ogoh S, Brothers RM, Hawkins M, Olivencia-Yurvati A, Raven PB.** Carotid baroreflex control of leg vasculature in exercising and non-exercising skeletal muscle in humans. *J Physiol* 561: 283–293, 2004.
25. **Leshnower BG, Potts JT, Garry MG, Mitchell JH.** Reflex cardiovascular responses evoked by selective activation of skeletal muscle ergoreceptors. *J Appl Physiol* 90: 308–316, 2001.
26. **Liu Z, Chen CY, Bonham AC.** Frequency limits on aortic baroreceptor input to nucleus tractus solitarii. *Am J Physiol Heart Circ Physiol* 278: H577–H585, 2000.
27. **Marmarelis PZ, Marmarelis VZ.** The white noise method in system identification. In: *Analysis of Physiological Systems*. New York: Plenum, 1978, p. 131–221.
28. **Matsukawa K, Nakamoto T, Inomoto A.** Gadolinium does not blunt the cardiovascular responses at the onset of voluntary static exercise in cats: a predominant role of central command. *Am J Physiol Heart Circ Physiol* 292: H121–H129, 2007.

29. **McIlveen SA, Hayes SG, Kaufman MP.** Both central command and exercise pressor reflex reset carotid sinus baroreflex. *Am J Physiol Heart Circ Physiol* 280: H1454–H1463, 2001.
30. **Melcher A, Donald DE.** Maintained ability of carotid baroreflex to regulate arterial pressure during exercise. *Am J Physiol Heart Circ Physiol* 241: H838–H849, 1981.
31. **Mense S, Stahnke M.** Responses in muscle afferent fibres of slow conduction velocity to contractions and ischaemia in the cat. *J Physiol* 342: 383–397, 1983.
32. **Miki K, Yoshimoto M, Tanimizu M.** Acute shifts of baroreflex control of renal sympathetic nerve activity induced by treadmill exercise in rats. *J Physiol* 548: 313–322, 2003.
33. **Miles R.** Frequency dependence of synaptic transmission in nucleus of the solitary tract in vitro. *J Neurophysiol* 55: 1076–1090, 1986.
34. **Mohrman DE, Heller LJ.** Regulation of arterial pressure. In: *Cardiovascular Physiology* (4th ed.). New York: McGraw-Hill, 1997, p. 158–230.
35. **Norton KH, Boushel R, Strange S, Saltin B, Raven PB.** Resetting of the carotid arterial baroreflex during dynamic exercise in humans. *J Appl Physiol* 87: 332–338, 1999.
36. **Ogoh S, Fisher JP, Dawson EA, White MJ, Secher NH, Raven PB.** Autonomic nervous system influence on arterial baroreflex control of heart rate during exercise in humans. *J Physiol* 566: 599–611, 2005.
37. **Ogoh S, Fisher JP, Fadel PJ, Raven PB.** Increases in central blood volume modulate carotid baroreflex resetting during dynamic exercise in humans. *J Physiol* 581: 405–418, 2007.
38. **Ogoh S, Fisher JP, Raven PB, Fadel PJ.** Arterial baroreflex control of muscle sympathetic nerve activity in the transition from rest to steady-state dynamic exercise in humans. *Am J Physiol Heart Circ Physiol* 293: H2202–H2209, 2007.
39. **Ogoh S, Wasmund WL, Keller DM, AOY, Gallagher KM, Mitchell JH, Raven PB.** Role of central command in carotid baroreflex resetting in humans during static exercise. *J Physiol* 543: 349–364, 2002.
40. **Papelier Y, Escourrou P, Gauthier JP, Rowell LB.** Carotid baroreflex control of blood pressure and heart rate in men during dynamic exercise. *J Appl Physiol* 77: 502–506, 1994.
41. **Papelier Y, Escourrou P, Helloco F, Rowell LB.** Muscle chemoreflex alters carotid sinus baroreflex response in humans. *J Appl Physiol* 82: 577–583, 1997.
42. **Potts JT, Hand GA, Li J, Mitchell JH.** Central interaction between carotid baroreceptors and skeletal muscle receptors inhibits sympathoexcitation. *J Appl Physiol* 84: 1158–1165, 1998.
43. **Potts JT, Li J.** Interaction between carotid baroreflex and exercise pressor reflex depends on baroreceptor afferent input. *Am J Physiol Heart Circ Physiol* 274: H1841–H1847, 1998.
44. **Potts JT, Mitchell JH.** Rapid resetting of carotid baroreceptor reflex by afferent input from skeletal muscle receptors. *Am J Physiol Heart Circ Physiol* 275: H2000–H2008, 1998.
45. **Potts JT, Shi XR, Raven PB.** Carotid baroreflex responsiveness during dynamic exercise in humans. *Am J Physiol Heart Circ Physiol* 265: H1928–H1938, 1993.
46. **Querry RG, Smith SA, Stromstad M, Ide K, Raven PB, Secher NH.** Neural blockade during exercise augments central command's contribution to carotid baroreflex resetting. *Am J Physiol Heart Circ Physiol* 280: H1635–H1644, 2001.
47. **Rowell LB, O'Leary DS.** Reflex control of the circulation during exercise: chemoreflexes and mechanoreflexes. *J Appl Physiol* 69: 407–418, 1990.
48. **Sato T, Kawada T, Inagaki M, Shishido T, Takaki H, Sugimachi M, Sunagawa K.** New analytic framework for understanding sympathetic baroreflex control of arterial pressure. *Am J Physiol Heart Circ Physiol* 276: H2251–H2261, 1999.
49. **Smith SA, Querry RG, Fadel PJ, Gallagher KM, Stromstad M, Ide K, Raven PB, Secher NH.** Partial blockade of skeletal muscle somatosensory afferents attenuates baroreflex resetting during exercise in humans. *J Physiol* 551: 1013–1021, 2003.
50. **Stebbins CL, Brown B, Levin D, Longhurst JC.** Reflex effect of skeletal muscle mechanoreceptor stimulation on the cardiovascular system. *J Appl Physiol* 65: 1539–1547, 1988.
51. **Sugimachi M, Imaizumi T, Sunagawa K, Hirooka Y, Todaka K, Takeshita A, Nakamura M.** A new method to identify dynamic transduction properties of aortic baroreceptors. *Am J Physiol Heart Circ Physiol* 258: H887–H895, 1990.
52. **Suzuki S, Ando S, Imaizumi T, Takeshita A.** Effects of anesthesia on sympathetic nerve rhythm: power spectral analysis. *J Auton Nerv Syst* 43: 51–58, 1993.
53. **Terui N, Masuda N, Saeki Y, Kumada M.** Activity of barosensitive neurons in the caudal ventrolateral medulla that send axonal projections to the rostral ventrolateral medulla in rabbits. *Neurosci Lett* 118: 211–214, 1990.
54. **Vatner SF, Braunwald E.** Cardiovascular control mechanisms in the conscious state. *N Engl J Med* 293: 970–976, 1975.
55. **Vatner SF, Franklin D, Braunwald E.** Effects of anesthesia and sleep on circulatory response to carotid sinus nerve stimulation. *Am J Physiol* 220: 1249–1255, 1971.
56. **Vatner SF, Franklin D, Van Citters RL, Braunwald E.** Effects of carotid sinus nerve stimulation on blood-flow distribution in conscious dogs at rest and during exercise. *Circ Res* 27: 495–503, 1970.
57. **Wray DW, Fadel PJ, Keller DM, Ogoh S, Sander M, Raven PB, Smith ML.** Dynamic carotid baroreflex control of the peripheral circulation during exercise in humans. *J Physiol* 559: 675–684, 2004.
58. **Yamamoto K, Kawada T, Kamiya A, Takaki H, Miyamoto T, Sugimachi M, Sunagawa K.** Muscle mechanoreflex induces the pressor response by resetting the arterial baroreflex neural arc. *Am J Physiol Heart Circ Physiol* 286: H1382–H1388, 2004.
59. **Yamamoto K, Kawada T, Kamiya A, Takaki H, Sugimachi M, Sunagawa K.** Static interaction between muscle mechanoreflex and arterial baroreflex in determining efferent sympathetic nerve activity. *Am J Physiol Heart Circ Physiol* 289: H1604–H1609, 2005.

Vascular Endothelial Growth Factor Receptor-1 Regulates Postnatal Angiogenesis Through Inhibition of the Excessive Activation of Akt

Jun-ichiro Nishi,* Tohru Minamino,* Hideyuki Miyauchi, Aika Nojima, Kaoru Tateno, Sho Okada, Masayuki Orimo, Junji Moriya, Guo-Hua Fong, Kenji Sunagawa, Masabumi Shibuya, Issei Komuro

Abstract—Vascular endothelial growth factor (VEGF) binds both VEGF receptor-1 (VEGFR-1) and VEGF receptor-2 (VEGFR-2). Activation of VEGFR-2 is thought to play a major role in the regulation of endothelial function by VEGF. Recently, specific ligands for VEGFR-1 have been reported to have beneficial effects when used to treat ischemic diseases. However, the role of VEGFR-1 in angiogenesis is not fully understood. In this study, we showed that VEGFR-1 performs "fine tuning" of VEGF signaling to induce neovascularization. We examined the effects of retroviral vectors expressing a small interference RNA that targeted either the VEGFR-1 gene or the VEGFR-2 gene. Deletion of either VEGFR-1 or VEGFR-2 reduced the ability of endothelial cells to form capillaries. Deletion of VEGFR-1 markedly reduced endothelial cell proliferation and induced premature senescence of endothelial cells. In contrast, deletion of VEGFR-2 significantly impaired endothelial cell survival. When VEGFR-1 expression was blocked, VEGF constitutively activated Akt signals and thus induced endothelial cell senescence via a p53-dependent pathway. VEGFR-$1^{+/-}$ mice exhibited an increase of endothelial Akt activity and showed an impaired neovascularization in response to ischemia, and this impairment was ameliorated in VEGFR-$1^{+/-}$ Akt$1^{+/-}$ mice. These results suggest that VEGFR-1 plays a critical role in the maintenance of endothelial integrity by modulating the VEGF/Akt signaling pathway. (*Circ Res*. 2008;103:261-268.)

Key Words: VEGF ■ Akt ■ senescence ■ p53

Angiogenesis involves the differentiation, proliferation, and migration of endothelial cells, leading to tubulogenesis and the formation of vessels.[1] One of the most important receptors for angiogenesis is the vascular endothelial growth factor (VEGF) receptor, which is a member of the receptor tyrosine kinase family.[2,3] VEGF receptor (VEGFR)-1 and VEGFR-2 are closely related receptor tyrosine kinases and have both common and specific ligands. VEGFR-1 has weaker kinase activity, whereas VEGFR-2 is a highly active kinase that stimulates a variety of signaling pathways and induces a broad range of biological responses. Despite its weak kinase activity, VEGFR-1 is essential for normal development and angiogenesis.[4] VEGFR-1 null mutant mice die in utero because of the overgrowth of endothelial cells and vascular disorganization.[5,6] In contrast, mice expressing the VEGFR-1 that lacks the tyrosine kinase domain develop a normal cardiovascular system,[7] suggesting that VEGFR-1 kinase activity might not be required for vascular development during embryogenesis and that VEGFR-1 may act as a decoy receptor. Consistent with this concept, selective activation of chimeric VEGFR-1 (in the absence of chimeric VEGFR-2)[8] or a VEGF mutant that binds to VEGFR-1 does not influence cell proliferation, migration, or survival in vitro.[9–11]

However, recent studies have demonstrated that the role of VEGFR-1 in postnatal angiogenesis is more complicated than was initially recognized. For example, treatment with placenta growth factor (PlGF), a specific ligand for VEGFR-1, was reported to promote angiogenesis in vitro[11,12] and in vivo.[13] Overexpression of PlGF also induced angiogenesis in tumors[14] and the skin.[15] It has been suggested that stimulation by PlGF induces the heterodimerization of VEGFR-1 with VEGFR-2, leading to transactivation of VEGFR-2 and the promotion of angiogenesis.[8,16,17] Another possible explanation for the positive effect of PlGF on angiogenesis is that it prevents VEGF from binding to VEGFR-1, thereby

Original received July 3, 2007; resubmission received February 18, 2008; revised resubmission received June 11, 2008; accepted June 16, 2008.

From the Department of Cardiovascular Science and Medicine (J.N., T.M., H.M., A.N., K.T., S.O., M.O., J.M., I.K.), Chiba University Graduate School of Medicine, Japan; PRESTO (T.M.), Japan Science and Technology Agency, Saitama, Japan; the Department of Physiology (G.-H.F.), University of Connecticut Health Center, Farmington; the Department of Cardiovascular Medicine (J.N., K.S.), Kyushu University Graduate School of Medical Sciences, Fukuoka, Japan; and the Department of Molecular Oncology (M.S.), Graduate School of Medicine and Dentistry, Tokyo Medical and Dental University, Japan.

*These authors contributed equally to this study.

Correspondence to Issei Komuro, MD, PhD, Department of Cardiovascular Science and Medicine, Chiba University Graduate School of Medicine, 1-8-1 Inohana, Chuo-ku, Chiba 260-8670, Japan. E-mail komuro-tky@umin.ac.jp

Circulation Research **is available at http://circres.ahajournals.org** **DOI: 10.1161/CIRCRESAHA.108.174128**

increasing the binding and activation of VEGFR-2. In other studies, PlGF was shown to protect against hyperoxic vascular damage in the retina without provoking retinal neovascularization.[18] These results suggest that VEGFR-1 can either positively or negatively regulate angiogenesis depending on the circumstances, but further studies are required to better understand the role of this receptor in postnatal angiogenesis.

In the present study, we examined the effects of VEGFR-1 deletion on angiogenesis by using the retroviral vector expressing a small interference RNA that targeted the VEGFR-1 gene. Deletion of VEGFR-1 markedly reduced endothelial cell proliferation and thus impaired angiogenesis. Likewise, VEGFR-$1^{+/-}$ mice exhibited an impaired neovascularization in response to ischemia. This impairment was restored by inhibiting the excessive activation of Akt by VEGF. These results suggest that VEGFR-1 plays a critical role in the maintenance of endothelial integrity by modulating the VEGF/Akt signaling pathway.

Materials and Methods

Short Hairpin Interference RNA Vectors

The mammalian retrovirus expression vector pSIREN-RetroQ (Clontech) was used to achieve the expression of short hairpin interference RNA (shRNA) in human endothelial cells.

Statistical Analysis

Data are shown as mean±SEM. Differences between groups were examined by Student *t* test or ANOVA followed by the Bonferroni procedure for comparison of means. Values of $P<0.05$ were considered statistically significant.

Results

Effect of VEGF Receptor Gene Silencing on Endothelial Cell Function

To elucidate the role of VEGFR-1 in angiogenesis, we constructed mammalian retroviral vectors expressing a short hairpin interference RNA that targeted either the VEGFR-1 gene (shVEGFR-1) or the VEGFR-2 gene (shVEGFR-2). Northern blot and Western blot analyses revealed that introduction of each construct into human umbilical vein endothelial cells caused effective and stable downregulation of the expression of the target molecule (Figure 1A and 1B, and supplemental Figure IA [available online at http://circres.ahajournals.org]). It is noted that either shVEGFR-1 or shVEGFR-2 did not affect VEGFR-2 or VEGFR-1 expression, respectively (Figure 1B, and supplemental Figure IA). We used two kinds of constructs for the following experiments and both of them achieved similar results. The nonsilencing control vector (shNega) was used as a control. After infected endothelial cells were purified by incubation with antibiotics, we performed the tube formation assay. Deletion of VEGFR-1 or VEGFR-2 significantly impaired tube formation compared with control cells (Figure 1C). We next examined the proliferative activity of infected cells. We seeded 2×10^5 infected cells into 100-mm dishes with VEGF-A on day 0 and counted cell number on day 3. Compared with shNega-infected control endothelial cells, both shVEGFR-1– and shVEGFR-2–infected cells showed significantly lower proliferation (Figure 1D). Deletion of VEGFR-1 caused more marked impairment of cell proliferation than deletion of VEGFR-2 (Figure 1D). This inhibitory effect of VEGFR-1 deletion was more evident when infected endothelial cells were subjected to long-term culture. Although VEGFR-2 deletion slightly reduced the lifespan of cells compared with that of control cells, VEGFR-1 deletion significantly shortened the lifespan of endothelial cells (Figure 1E). As a result, shVEGFR-1–infected cells underwent irreversible growth arrest earlier than shVEGFR-2-infected cells (Figure 1E). After growth arrest, the cells exhibited characteristics of senescence, becoming flatter and larger and showing an increase of senescence-associated β-galactosidase activity (Figure 1F). These findings suggest that VEGFR-1 deletion induces premature endothelial cell senescence. We next examined the effect of VEGFR-1 deletion on endothelial survival. We cultured infected cells in regular growth medium for 24 hours and subsequently cultured the cells under serum-free conditions with VEGF-A. After 24 hours, the number of viable cells was counted. As compared with the viability of control cells, deletion of VEGFR-2, but not VEGFR-1, markedly decreased cell viability (Figure 1G). Consistent with these findings, activation of caspase 3 was detected in cells with VEGFR-2 deletion, but not VEGFR-1 deletion (Figure 1H). These results suggest that VEGFR-1 is involved in the regulation of angiogenesis by regulating endothelial cell proliferation and senescence, whereas VEGFR-2 may be crucial for endothelial survival as well as cell proliferation.

VEGFR-1 Deletion Induces Endothelial Dysfunction by Activating Akt

To investigate the molecular mechanisms of premature senescence induced by VEGFR-1 deletion, we examined the transcriptional activity of p53 and its target gene p21. We transfected VEGFR-1–deleted endothelial cells with the luciferase reporter gene containing 13 copies of the p53-binding consensus sequence (pPG13-Luc). Deletion of VEGFR-1 significantly induced p53 transcriptional activity compared with that in shNega-infected cells, whereas VEGFR-2 deletion had no effect (Figure 2A). Likewise, p21 expression was significantly higher in VEGFR-1–deleted endothelial cells than in control cells or VEGFR-2–deleted cells (Figure 2B). However, expression of bax, another target molecule regulated by p53, was not altered in VEGFR-1–deleted endothelial cells compared with control cells (supplemental Figure IB). Ablation of p53 by the introduction of HPV16 E6 oncoprotein abolished the inhibitory effect of VEGFR-1 deletion on cell proliferation (Figure 2C). These results suggest that VEGFR-1 deletion induces endothelial cell senescence via a p53-dependent pathway.

We have previously demonstrated that Akt negatively regulates the endothelial cell lifespan by activating the p53/p21 pathway.[19] It has also been shown that Akt plays a central role in the regulation of angiogenesis by VEGF.[20] Thus, we examined the level of phosphorylated Akt in VEGFR-1-deleted endothelial cells. Western blot analysis

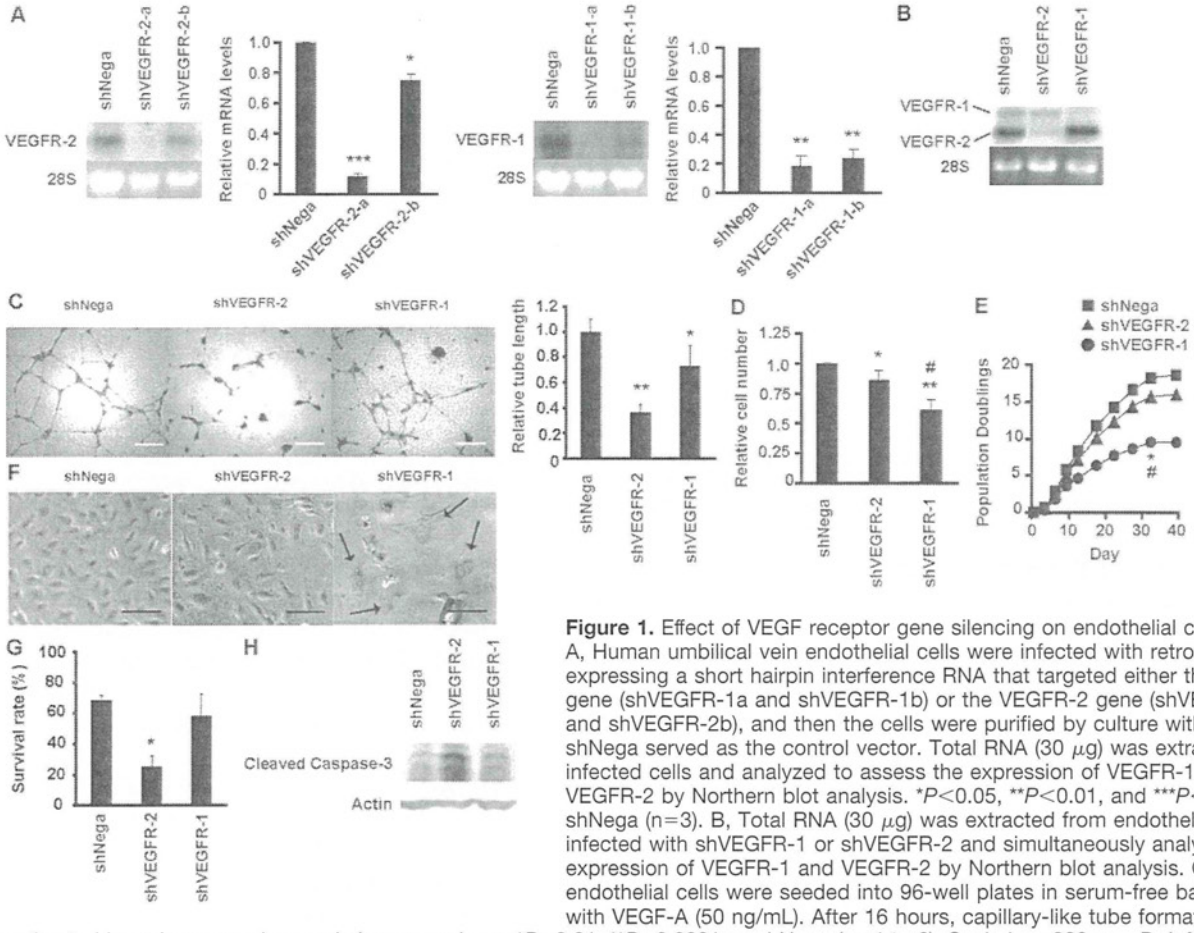

Figure 1. Effect of VEGF receptor gene silencing on endothelial cell function. A, Human umbilical vein endothelial cells were infected with retroviral vectors expressing a short hairpin interference RNA that targeted either the VEGFR-1 gene (shVEGFR-1a and shVEGFR-1b) or the VEGFR-2 gene (shVEGFR-2a and shVEGFR-2b), and then the cells were purified by culture with antibiotics. shNega served as the control vector. Total RNA (30 μg) was extracted from infected cells and analyzed to assess the expression of VEGFR-1 or VEGFR-2 by Northern blot analysis. *P<0.05, **P<0.01, and ***P<0.001 vs shNega (n=3). B, Total RNA (30 μg) was extracted from endothelial cells infected with shVEGFR-1 or shVEGFR-2 and simultaneously analyzed the expression of VEGFR-1 and VEGFR-2 by Northern blot analysis. C, Infected endothelial cells were seeded into 96-well plates in serum-free basic medium with VEGF-A (50 ng/mL). After 16 hours, capillary-like tube formation was estimated by using an angiogenesis image analyzer. *P<0.01, **P<0.0001 vs shNega (n=4 to 6). Scale bar: 300 μm. D, Infected endothelial cells were seeded at a density of 2×10^5 cells per 100-mm dish and cultured with VEGF-A (day 0). Then cell number was counted on day 3. *P<0.001, **P<0.0001 vs shNega, #P<0.001 vs shVEGFR-2 (n=13 to 14). E, Infected cell populations were passaged until cells underwent senescence, and the total number of population doublings was determined. *P<0.01 vs shNega, #P<0.05 vs shVEGFR-2 (n=4 to 6). F, Morphology and senescence-associated β-galactosidase staining (arrow) of endothelial cells infected with shNega, shVEGFR-1, or shVEGFR-2. Scale bar: 100 μm. G, Infected endothelial cells were seeded at the density of 1×10^5 cells per 60-mm dish and cultured for 24 hours in growth medium. After washing twice with PBS, the cells were cultured in serum-free DMEM with VEGF-A (10 ng/mL). After 24 hours of serum starvation, the number of viable cells and the total number of cells were counted by a hemocytometer. *P<0.0001 vs shNega (n=4 to 6). H, The lysates were extracted from cells, which are prepared as described in legend for G, and analyzed for cleaved caspase-3 expression by Western blotting.

showed that VEGFR-1 deletion led to a marked increase of the phosphorylated Akt level compared with that in control cells or cells with VEGFR-2 deletion, even under serum-free conditions (Figure 3A). VEGFR-1 deletion increased pAkt levels even in the absence of VEGF, presumably attributable to autocrine VEGF signaling (Figure 3B). Treatment with VEGF markedly increased pAkt levels within 5 to 15 minutes in VEGFR-1–deleted cells but not in VEGFR-2–deleted cells (Figure 3B). Treatment with a neutralizing anti-VEGF antibody reduced the phosphorylated Akt level in VEGFR-1-deleted cells (Figure 3C), suggesting that VEGFR-1 inhibits the activation of Akt by VEGF. To further investigate the relationship between constitutive Akt activation and endothelial cell dysfunction induced by VEGFR-1 deletion, we examined the effect of inhibition of Akt. We infected human endothelial cells with a retroviral vector encoding a dominant-negative form of Akt (DN-Akt)[19] or the empty vector encoding resistance to neomycin alone (Mock). Both cell populations were then infected with shNega or shVEGFR-1. We found that VEGFR-1 deletion markedly inhibited the proliferation of mock-infected endothelial cells (Figure 3D, Mock), whereas this inhibitory effect was significantly ameliorated in DN-Akt–infected cells (Figure 3D, DN-Akt). Consequently, VEGFR-1 deletion significantly impaired tube formation by mock-infected cells, but not DN-Akt-infected cells (Figure 3E). Likewise, inhibition of Akt activation prevented the induction of p21 expression by VEGFR-1 deletion (supplemental Figure II). These results suggest that VEGFR-1 deletion causes dysregulation of activation of the VEGFR-2/Akt signaling pathway by VEGF-A, and that constitutive activation of Akt is related to the impaired ability of VEGFR-1–deleted endothelial cells to proliferate and form capillary-like structures. VEGF-induced phosphorylation of eNOS was enhanced, but production of cGMP was significantly reduced by VEGFR-1 deletion, presumably because constitutive activation of Akt increases cellular reactive oxygen species[19] that inactivate this enzyme (supplemental Figure IC and ID).